npj computational materials

www.nature.com/npjcompumats

ARTICLE OPEN

Driving forces for ultrafast laser-induced sp^2 to sp^3 structural transformation in graphite

Chenchen Song[1,2,5], Mengxue Guan[1,2,4,5], Yunzhe Jia[1,2], Daqiang Chen[1,2], Jiyu Xu[1,2], Cui Zhang[1,3]✉ and Sheng Meng[1,2,3]✉

Understanding the microscopic mechanism of photoinduced sp^2-to-sp^3 structural transformation in graphite is a scientific challenge with great importance. Here, the ultrafast dynamics and characteristics of laser-induced structural transformation in graphite are revealed by non-adiabatic quantum dynamic simulations. Under laser irradiation, graphite undergoes an interlayer compression and sliding stage, followed by a key period of intralayer buckling and interlayer bonding to form an intermediate sp^2-sp^3 hybrid structure, before completing the full transformation to hexagonal diamond. The process is driven by the cooperation of charge carrier multiplication and selective phonon excitations through electron-phonon interactions, in which photoexcited hot electrons scattered into unoccupied high-energy conduction bands play a key role in the introduction of in-plane instability in graphite. This work identifies a photoinduced non-adiabatic transition pathway from graphite to diamond and shows far-reaching implications for designing optically controlled structural phase transition in materials.

npj Computational Materials (2023)9:76 ; https://doi.org/10.1038/s41524-023-01035-2

INTRODUCTION

Ultrafast laser has a wide range of applications in controlling the structures and properties of materials[1–4]. In recent years, photo-induced structural phase transitions have attracted great attentions[4–7]. Carbon, one of the most important elements in nature, can form a large number of organic and inorganic substances, of which its elements can exist in various forms, such as 0-dimensional (0D) C_{60} nanoclusters, 1D carbon nanotubes, (quasi-)2D graphene and graphite, and 3D diamond. The manipulation of the sp, sp^2, and sp^3 hybridized bonds provides a rich opportunity to study the structural transition of their allotropes and thus to tune the corresponding electronic and optical properties. Graphite and diamond are the most stable crystalline solid phases at atmospheric pressure and high pressure, respectively. Graphite is a prototype layered crystal with strong in-plane sp^2 hybridized covalent bonds and weak interlayer van der Waals interactions, while diamond is composed of pure sp^3 hybridized bonds. Although the thermodynamic energies of the two structures are nearly identical, the conversion from graphite to diamond is highly challenging, which requires extreme conditions such as high temperature, high pressure or laser pulses[8–14].

At ambient temperature and pressure, it has reported that graphite can form sp^3-bonded structure under intense femtosecond laser irradiation[11–14]. Raman et al. found that when the laser fluence is close to the damage threshold of graphite, interlayer bonds are formed after a significant contraction of interlayer spacing[11]. According to their density functional theory (DFT) calculations, the modified force field due to changes in charge density and the Coulomb stress produced by the photoinduced charge separation are the main forces driving the structural change in graphite. Kanasaki et al. showed that after the exposure of intense laser pulses, the structural periodicity of sp^3-bonded carbon nanodomains differs from that of conventional diamond[12], indicating that the laser-driven phase transition is distinct from that under high pressures[9,15]. Classical molecular dynamics simulations with semi-empirical potentials indicated a nonlinear relationship between the number of photoexcited carbon sites and the number of interlayer bonds formed in graphite[16,17]. Nüske et al. observed the formation of nanoscale cubic diamond crystals in the laser-irradiated highly oriented pyrolytic graphite (HOPG) sample using Raman spectroscopy[13]. Duan et al. showed that sp^2-sp^3 transformation in twisted bilayer graphene occurs under femtosecond laser irradiation, where the moiré pattern plays an important role[14]. These studies mainly detected the photoinduced structural changes in the samples by various means, to demonstrate the achievement of sp^2-sp^3 transformation in graphite by femtosecond laser action. Some of these measurements directly showed the interlayer contraction before the formation of interlayer bonds. However, the spatial and temporal resolution of the structure transformation process is rough, and the exploration of the non-equilibrium carrier dynamics in graphite is lacking. In addition, light-induced carbon phase transformations evolve on extremely non-equilibrium paths at ultrafast time-scales, and therefore it is crucial to consider and understand the ultrafast dynamics of photoexcited charge carriers in the process, which involves weakly screened carrier-carrier scatterings and carrier-phonon interactions[18–20]. Due to the lack of accurate description of strong-field-driven photocarrier dynamics and understanding of the key mechanisms underlying such extreme non-equilibrium phase transformations, the microscopic dynamic picture of the photoinduced sp^2-to-sp^3 structural transition remains an intriguing open problem.

In the present work, we reveal the pathway and mechanism of laser-induced structural transformation of graphite at the microscopic and ultrafast scales, using non-adiabatic molecular dynamics calculations within the framework of real-time time-dependent density functional theory (rt-TDDFT). Our results

[1]Beijing National Laboratory for Condensed Matter Physics and Institute of Physics, Chinese Academy of Sciences, 100190 Beijing, China. [2]School of Physical Sciences, University of Chinese Academy of Sciences, 100049 Beijing, China. [3]Songshan Lake Materials Laboratory, 523808 Dongguan, Guangdong, China. [4]Present address: Centre for Quantum Physics, Key Laboratory of Advanced Optoelectronic Quantum Architecture and Measurement (Ministry of Education), School of Physics, Beijing Institute of Technology, 100081 Beijing, China. [5]These authors contributed equally: Chenchen Song, Mengxue Guan. ✉email: cuizhang@iphy.ac.cn; smeng@iphy.ac.cn

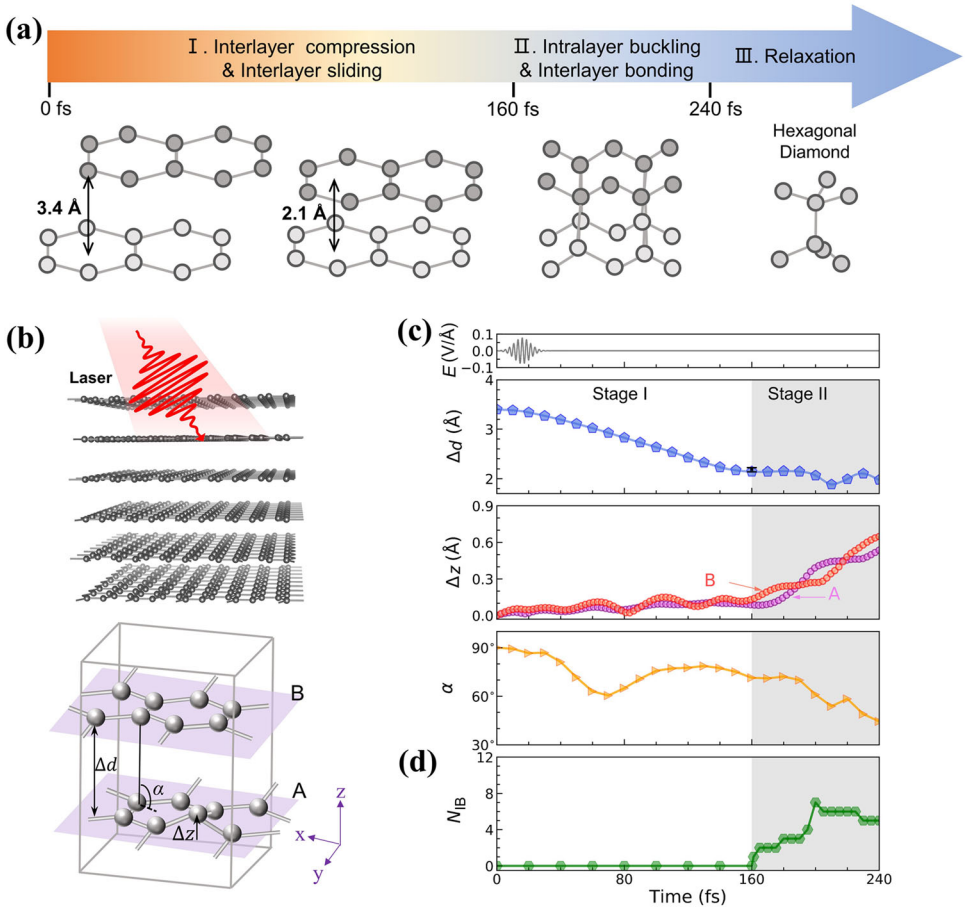

Fig. 1 Photoinduced sp^2-to-sp^3 structural transformation process in graphite. a Schematic of three-stage ultrafast laser-induced structural transformation in graphite. **b** Atomic structure of AB stacked graphite used in the non-adiabatic first-principles simulations of ultrafast laser-induced sp^2-to-sp^3 structural transformation. **c** Time evolution of the laser field waveform, the interlayer spacing Δd, the intralayer buckling height Δz and interlayer sliding angle α of graphite. The α is defined as the angle formed by the carbon pairs located in the same x-y position of adjacent layers with respect to the layer plane. The Gaussian-shaped laser pulse is polarized along the armchair direction of graphite with a field strength of $E_0 = 0.077$ V Å^{-1} and a fluence of $F = 0.905$ mJ cm^2. The pulse width and the photon energy are 10 fs and 1.55 eV, respectively. The laser field reaches the maximum strength E_0 at time t_0=16 fs. **d** Time evolution of the number of interlayer bonds (N_{IB}) formed in the laser-induced sp^2-to-sp^3 structural transformation process.

identify three consecutive stages for the laser-induced sp^2-to-sp^3 bond transformation in graphite on the ultrafast time-scale, as illustrated in Fig. 1a. Under laser excitation, the interlayer spacing of graphite undergoes rapid compression, attributed to the photoinduced reduction of charge population in the $2p_z$ orbital. Specific phonon modes, e.g., E^1_{2g}, B_{2g} and E^2_{2g}, are excited to promote the interlayer sliding and structural deformation. Subsequently, interlayer bonds are gradually formed through the buckling of carbon atoms in adjacent layers. The initial layered structure with in-plane sp^2 bonding is then transformed into an intermediate structure containing both sp^2 and sp^3 bonds. We find that structural transformation process, including interlayer compression and bonding, is driven by the cooperation of charge carrier multiplication and selective phonon excitations through electron-phonon interactions. The high-energy intermediate state may reach thermal equilibrium through complex electron-phonon and phonon-phonon collisions into hexagonal diamond (HD) structure.

RESULTS AND DISCUSSION

Photoinduced sp^2-to-sp^3 structural transformation

We apply an ultrafast laser pulse with a photon energy of 1.55 eV on the graphite crystal along the armchair direction. To characterize the structural transformation of graphite under laser irradiation, we analyze two types of atomic displacements, i.e., interlayer spacing Δd and intralayer buckling height Δz, as illustrated in Fig. 1b. The Gaussian-shaped laser pulse with a maximum strength of $E_0 = 0.077$ V Å^{-1} at 16 fs, as well as the time variation of structural parameters Δd and Δz at a laser fluence of $F = 0.905$ mJ cm^{-2} are presented in Fig. 1c. The interlayer spacing Δd of graphite rapidly decreases from 3.4 Å to 2.14 Å (Stage I) under laser action. After significant interlayer shrinkage, the layer spacing stabilizes. As the carbon atoms of the adjacent layers get closer, the out-of-plane distortion Δz of the atoms in layer A and B increases remarkably after 160 fs (Stage II). Along with the decrease of the layer spacing and the increase of buckling height, the interlayer sliding angle α, defined as the angle formed by the carbon pairs located in the same x-y position of adjacent layers with respect to the layer plane, continues to reduce, showing that the two layers of graphite also undergo significant sliding.

We further define the formation of interlayer bonds as the distance between pairs of carbon atoms of adjacent layers is less than 2.0 Å and show the number of formed interlayer bonds (N_{IB}) as a function of time in Fig. 1d. The variation of Δz and N_{IB} with time clearly show that the intralayer buckling of carbon atoms effectively promotes the formation of interlayer bonds, implying the appearance of intermediate states containing sp^2 and sp^3

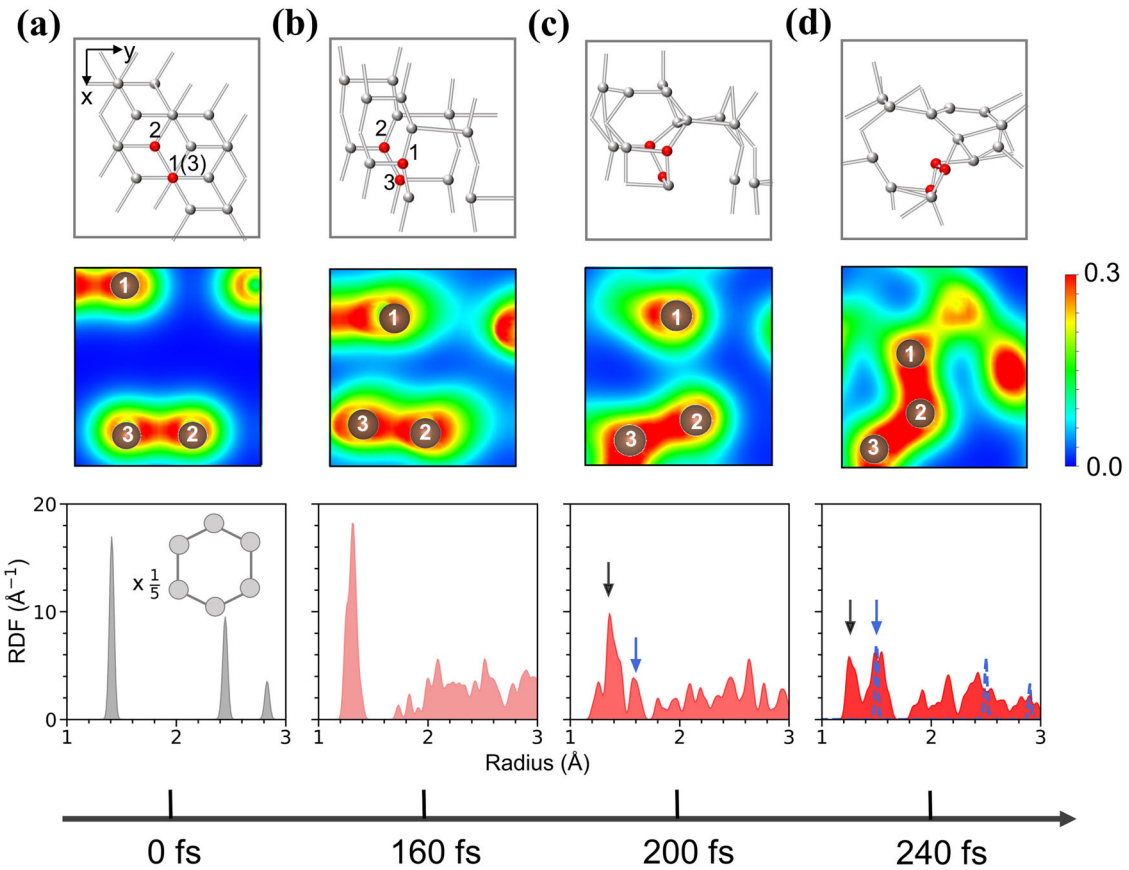

Fig. 2 Structural changes during the phase transition. Atomic configuration, local charge density and corresponding RDF of graphite upon laser irradiation at **a** 0 fs, **b** 160 fs, **c** 200 fs, and **d** 240 fs, respectively. Carbon pairs located at the same site in *x-y* plane but adjacent layers are labeled as C_1 and C_3, and the atom next to C_3 within the same hexagon is labeled as C_2. The cross-section of the charge density contour is a plane including all three atoms. The unit for charge density contour is e bohr^{-3}. The black and blue arrows are used to indicate the characteristic peak positions of sp^2 and sp^3 hybridized bonds in the RDF, respectively, and the blue dashed lines represent the peak positions of HD.

bonds. The structural deformation characteristics of graphite under laser illumination, i.e., the formation of interlayer bonds after significant interlayer compression and sliding, are consistent with the previous experimental observations[11]. We have performed three different independent simulations initiated with the same laser parameter settings over a random distribution. As shown in Supplementary Fig. 1, the light-induced structural transitions occurred in graphite are consistent with each other quantitatively.

We show in Fig. 2 the changes in graphite atomic configurations at representative moments in the photoinduced phase transformation pathway, along with the corresponding local charge density and radial distribution function (RDF). Upon photoexcitation, interlayer contraction and sliding of AB stacked graphite, result in the shift and broadening of RDF peaks within 160 fs (stage I), which is also related to the transient deformation of the honeycomb lattice. To 200 fs, the amplitude of the sp^2 characteristic peak position continues to decrease, accompanied by the appearance of a peak near 1.6 Å, indicated by the black and blue arrows in Fig. 2c, respectively. At the end of stage II (240 fs), two peaks with comparable amplitude are formed, indicating the appearance of an intermediate state consisting of sp^2 and sp^3 hybridized bonds. At this point, the density of transformed structure reaches 3.29 g cm^{-3}, which is close to the density of HD (3.51 g cm^{-3})[21], compared to the density of graphite (2.24 g cm^{-3}). The RDF at 240 fs shows a hybrid structure that includes the HD structure (the characteristic peak of HD shown as blue dashed lines in Fig. 2d), therefore, the system continues to the structural relaxation stage (stage III) before the complete transformation to HD.

Selective excitation of multiple phonons

Previous studies have demonstrated that more than 90% of the absorbed laser energy in graphite is transferred from the electronic system into several strongly coupled optical phonons within the first 500 fs after excitation, including E^2_{2g} mode at the Γ point and A'_1 mode at the K point[22–25]. Here we focus on the phonon excitation of the Γ point and calculate all forty-eight eigenvectors of phonons. Time evolution of each phonon branch is explored by projecting the displacement of atoms in the trajectory onto forty-eight phonon eigenvectors. The projected intensity is defined as $\frac{1}{\sqrt{m}}\sum_j \mathbf{e_i} \bullet \mathbf{u_j}$, where m is the mass of the carbon atoms, $\mathbf{u_j}$ is the displacement vector of atom j from its original position at $t = 0$, and $\mathbf{e_i}$ is the ith phonon eigenvector at the Γ point. As shown in Fig. 3a, we find that in addition to the strongly coupled stretching mode E^2_{2g} (1602.20 cm^{-1}), E^1_{2g} (46.86 cm^{-1}) and B_{2g} (130.82 cm^{-1}) are the other two phonon modes intensely excited by the laser. These three phonon modes excited within 160 fs dominate the photoinduced structural transformation of graphite. The vibrational modes of three excited phonons are shown in Fig. 3b. The interlayer shearing mode E^1_{2g} is associated with interlayer sliding, which has been experimentally found to be generated mainly by the real excitation of the π-π* optical transition[26]. Moreover, the optically inactive B_{2g} mode is associated with interlayer compression. The electronic energy

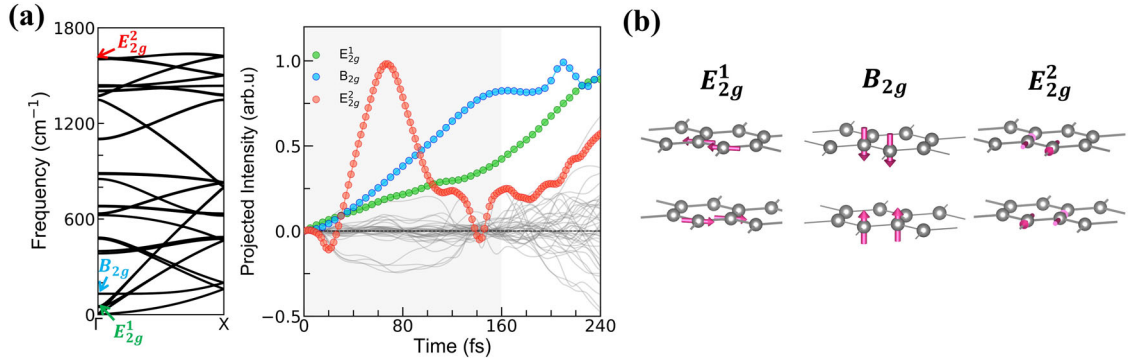

Fig. 3 Selective excitation of multiple phonons. a Phonon dispersion spectrum and time evolution of all forty-eight Γ-point projected phonon branches in graphite. Three excited phonons are E^1_{2g}, B_{2g}, and E^2_{2g} modes. **b** Vibrational modes of three excited phonons. The pink arrows indicate the direction of relative motions of the atoms.

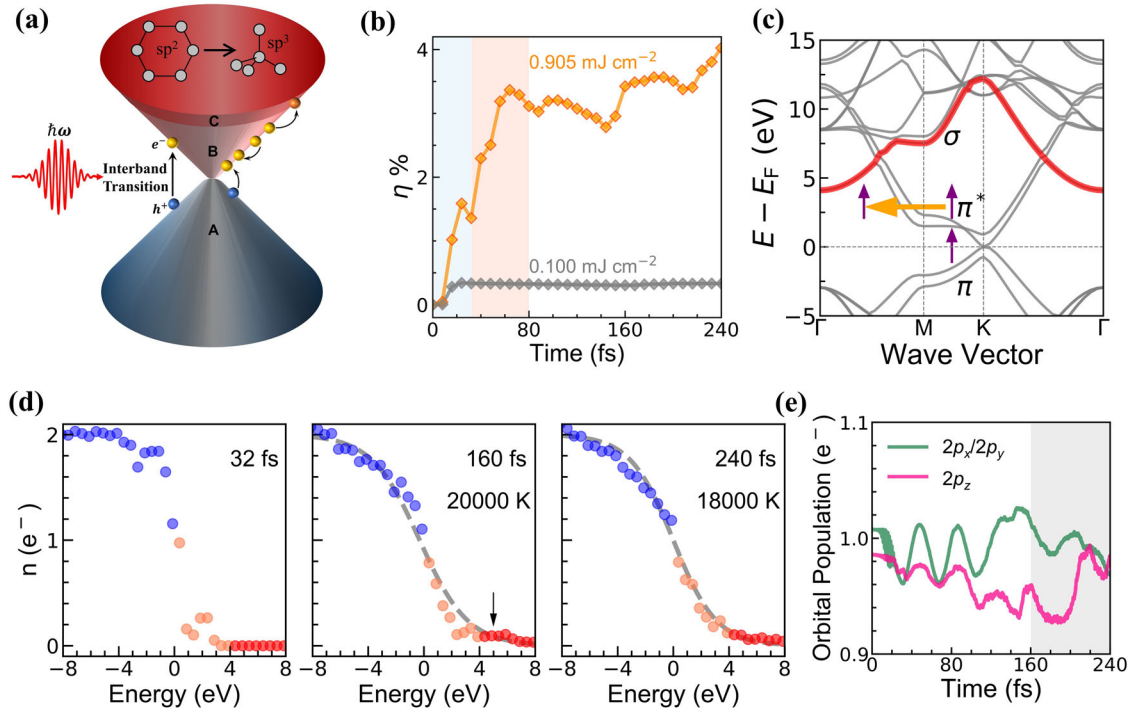

Fig. 4 Electronic excitation. a Schematic diagram of the photogenerated carrier transport process in the structural transformation of graphite. Region A: valence bands ($E \le E_F$); Region B: low-energy region in the conduction bands ($E_F < E < 4$ eV); Region C: high-energy region in the conduction bands ($E \ge 4$ eV). **b** The percentage of excited electrons (η%) under photoexcitation at a fluence $F = 0.905$ mJ cm^{-2} and $F = 0.100$ mJ cm^{-2}. Blue and coral areas indicate the laser direct action stage (0–32 fs) and the carrier multiplication stage (32–80 fs). **c** Band structure of graphite with the electronic transition process between bands is illustrated by arrows. The red line denotes the unoccupied σ interlayer band. **d** The electron distributions at the end of laser action (32 fs), stage I (160 fs) and stage II (240 fs), under strong excitation ($F = 0.905$ mJ cm^{-2}). The blue, coral, and red dots are used to present the distribution of electrons in the energy regions of A, B, and C depicted in panel **a**. The electronic temperature T_e is obtained by fitting the Fermi-Dirac function (dash line). The Fermi level E_F is set to 0 eV. **e** Time evolution of charge population for $2p_x$, $2p_y$, and $2p_z$ orbitals from Mulliken charge analysis upon intense photoexcitation at a fluence $F = 0.905$ mJ cm^{-2}.

obtained from photon absorption is transferred to only a few specific phonon modes in stage I, leading to structural instability, including interlayer compression and sliding. Such selective phonon excitations via electron-phonon coupling are further coupled to other vibrations after 160 fs (stage II), accompanied by sp^2-to-sp^3 bond conversion.

Electronic driving forces

After clarifying the selective mechanism of multiple phonon excitation induced by photoexcited electrons through the strong electron-phonon couplings, we further elaborate the underlying electronic driving forces in such photoinduced phase transition in graphite, as illustrated in Fig. 4a. We first trace the number of excited electrons in graphite upon the photoexcitation at a fluence of 0.905 mJ cm^{-2}. The time variation of the percentage of excited electrons indicates a significant carrier multiplication stage (coral shaded region in Fig. 4b). In the period of laser direct action (0–32 fs, blue shaded region in Fig. 4b), electrons are excited from the valence to conduction bands of graphite, with an equal number of holes generated in the valence bands. The number of excited electrons continues to increase for a period of time (32–80 fs) after the laser pulse ends. Such carrier multiplication

effect has been explored in graphite materials[27–31] and can induce nonthermal ultrafast phase transitions in semiconductors[32]. Carrier multiplication is the result of a stronger effect of impact ionization than Auger recombination. Impact ionization process, by which electrons with sufficient energy in conduction band relax to generate new electron-hole pairs, leads to an increase in the carrier density, as depicted in Fig. 4a. Whereas, the Auger recombination involves the scattering of two electrons and electron-hole recombination, resulting in the decrease of carrier density. We observed carrier multiplication in graphite under strong excitation capable of triggering the formation of sp^3 bonds, but not under weak excitation that fails to induce the structural transformation, as shown in Fig. 4b and Supplementary Fig. 2. Since adiabatic TDDFT tends to underestimate the scattering and energy-transfer in real systems to some extent, the real impact ionization process may be stronger than our simulation results.

After carrier multiplication period, the percentage of excited electrons maintains at about 3.5% per supercell and the system continues to evolve. Small portion of high-energy electrons (HEs) are scattered to the σ interlayer band, which is essential for the sp^2-to-sp^3 bond conversion. It has been demonstrated that there exists a σ-symmetry interlayer band with 3D free-electron features and the band minimum at the Γ point is about 4.0 eV above the Fermi level[33,34]. The electrons can be transferred from the π^* bands (B region in Fig. 4a) to the unoccupied σ interlayer band by electronic relaxation, as illustrated in Fig. 4c. Previous study has proposed that such a redistribution of electrons leads to lattice instability by weakening the in-plane C=C bonds and promotes out-of-plane distortions[35]. Thus, the HEs scattered into the unoccupied σ interlayer band drive the out-of-plane distortion and trigger the formation of interlayer bonds.

We further analyze in Fig. 4d the electron distribution upon intense photoexcitation ($F = 0.905\ \mathrm{mJ\,cm^2}$) at the end of laser action, stage I and stage II, respectively. At the end of ultrafast laser irradiation, the photogenerated electron-hole pairs are mainly distributed in an energy range near the Fermi level ($|E - E_F| < 4$ eV). A small amount of the excited electrons is scattered to high-energy conduction bands (C region: $E - E_F \geq 4$ eV) during the electronic relaxation, as pointed out by the arrow in Fig. 4d. To estimate the electronic temperature T_e at different moments, we use the Fermi-Dirac (FD) function $g(E) = \left(e^{\frac{E-\mu}{kT_e}} + 1\right)^{-1}$ to fit the distribution of electrons, where μ represents the chemical potential and k is the Boltzmann constant. At 160 fs, when the interlayer sp^3 bonds begin to form, T_e is about 20,000 K. The electron-phonon interaction leads to the transfer of energy from the electronic system to the lattice structure, resulting an effective T_e of 18,000 K at 240 fs. It predicts a longer period of thermal relaxation to further transform into a perfect diamond structure (stage III).

Furthermore, the Mulliken charge analysis allow us to track the time evolution of the charge population for carbon $2p_x$, $2p_y$, and $2p_z$ orbitals, shown in Fig. 4e. The ultrafast laser induces a continuous decrease in the charge population of the $2p_z$ orbital over 160 fs, which is responsible for the interlayer contraction. In stage II, that is, the period of sp^3 bond formation, the charge population of the $2p_x$, $2p_y$, and $2p_z$ orbitals gradually tend to be equal, indicating a weakening of the anisotropy of bonding orbitals that facilitates the transition to sp^3 hybridization.

Mechanism of photoinduced sp^2-to-sp^3 structural transformation

We have identified the microscopic dynamic process of ultrafast laser-induced graphite structural transformation, which is characterized by three main stages, as illustrated in Fig. 1a. Within the first stage, a large number of electrons are excited to the conduction bands of graphite through optical absorption and carrier multiplication, and then redistributed. Attributed to electron-phonon interactions, several specific phonons are excited in graphite, resulting in rapid interlayer sliding and contraction. The change in graphite layer stacking pattern is an intermediate state before conversion to diamond, as indicated in previous studies[15,36]. The compressed transient state at the end of the first stage is metallic (Supplementary Fig. 3b), with 2.37 eV per atom higher energy than graphite. We also note that high laser fluence is essential to achieve such irreversible compression (Supplementary Fig. 2), while it does not show a strong correlation with the laser wavelength (Supplementary Fig. 4).

The second stage is the buckling of carbon atoms in adjacent layers, which promotes the formation of interlayer bonds (160–240 fs). We suggest that the HEs play a key role in the sp^2-to-sp^3 bonding transition. Along with the structural transformation, the electrons tend to obey the FD distribution with a high electron temperature due to carrier relaxation. Although the system has a density similar to HD at 240 fs, with a band gap of 0.3 eV (Supplementary Fig. 3c), it has not been fully converted to HD. The energy of the structure is still higher than that of the graphite by 1.22 eV per atom. Therefore, in the third stage (after 240 fs), further structural relaxation is required to transform the atomic structure into a perfect HD with a wide band gap (Supplementary Fig. 3d) and lower energy (0.013 eV per atom higher than graphite).

Recent studies on direct transformation from graphite to diamond under high pressure and temperature have reported the identification of nanoscale coherent graphite-diamond interfaces at which the graphite and diamond units are bonding each other[10]. The transformation has been shown to occur in the two stages, namely the formation of coherence interface and the subsequent advances of the interface. In contrast to the clear graphite-to-diamond transformation process under high pressure, the microscopic formation process of the sp^3-bonded structures upon photoexcitation has not been clearly revealed by experiments[11,12]. Our studies propose the underlying mechanism of ultrafast structural transformation in graphite driven by the cooperation of photoexcited charge carrier multiplication and selective phonon excitation, forming hybrid structures as seeds for further evolution. The hybrid structures including both sp^2 and sp^3 types of bonding are not identical to the nanoscale coherent interfaces found in ref. [10], but both share the same intermediate state characteristics. The non-equilibrium phonon dynamics suggested in our studies can be observed experimentally by monitoring the diffraction intensity evolution of the Bragg peak using the ultrafast electron diffuse scattering (UEDS) tools, as indicated in Supplementary Fig. 5. The ultrafast photoinduced structural transformation observed in twisted bilayer graphene is revealed by the reduction in the diffraction intensity and momentum transfer vector within ~330 fs[14], consistent with the non-equilibrium dynamics time-scale reported in our study.

In summary, our first-principles non-adiabatic dynamics simulations reveal the pathway and mechanism of ultrafast photo-induced structural transformation of graphite to diamond mediated by a hybrid structure of sp^2 and sp^3 bonds. Upon intense laser irradiation, the underlying driving forces of such process are the carrier multiplication of excited electrons through electron-electron interactions and the specific phonon excitation due to electron-phonon couplings. Graphite undergoes a structural transformation of interlayer compression, sliding, interlayer buckling and sp^3 bond-forming on ultrafast time-scales. The presence of photoexcited electrons in the unoccupied σ interlayer bands plays a key role in the sp^2-to-sp^3 bond conversion. Our findings provide a plausible non-adiabatic mechanism for light-induced graphite-to-diamond conversion from an electronic perspective and also offer an atomistic insight into the control of the phase transitions in quantum materials by ultrafast laser excitation. Such optically controlled approach has a great potential for applications in many fields, such as nanostructure processing, optical memory, and device fabrication.

METHODS

Non-adiabatic molecular dynamic simulations

The non-adiabatic molecular dynamics (NAMD) simulations based on rt-TDDFT are performed using the time-dependent ab initio package (TDAP), which provides an efficient method for tracking real-time dynamics of complicated processes in the excited states[37,38]. Graphite crystal is simulated with a $2\times\sqrt{3}\times 1$ supercell, containing two sublayers (A, B) of 16 carbon atoms with periodical boundary condition. The initial lattice dimensions of the supercell are 4.92 Å, 4.26 Å, and 6.80 Å, respectively. We adopt a numerical atomic orbital basis set with double zeta polarization (DZP) and Troullier-Martins pseudopotentials, with an auxiliary real-space grid equivalent to a plane-wave cutoff of 150 Ry. The Brillouin zone of unit cell is sampled by a $4\times4\times3$ ***k***-mesh. The exchange and correlation energy is treated within the local density approximation (LDA)[39]. We apply a linearly polarized laser field with a Gaussian envelope $E(t) = E_0\cos(\omega t)\exp[-(t-t_0)^2/2\sigma^2]$ to excite the graphite crystal. The time step of 40 attoseconds is applied for both electron and ion motions, evolving in a constant-pressure-energy (NPE) ensemble. The coupling between atomic and electronic motions is described by the Ehrenfest approximation. The pressure is controlled by Parrinello-Rahman method[40] and no symmetry is constrained for either the supercell shape or the atomic positions. Partial phonon-phonon interactions such as optical phonon-phonon interactions are included, but some dissipation channels such as acoustic phonon-phonon interactions, are not considered due to the limitation of cell size. Energy dissipation mediated by phonon-phonon interactions typically occurs on relatively slow time-scales (>1 ps), and given the focus of our work on the ultrafast dynamics of structural transitions occurring within a few hundred femtoseconds, such short time-scale dynamics (<1 ps) is not qualitatively affected by supercell dimensions.

Band structure and phonon calculations

DFT calculations were performed by Vienna Ab Initio Simulation Package (VASP)[41] using the projector augmented wave (PAW)[42] method and LDA for the exchange-correlation energy. Phonon calculations are performed using the finite displacement method within the PHONOPY[43].

DATA AVAILABILITY

The data that support the findings of this work are available from the corresponding author upon reasonable request.

CODE AVAILABILITY

Rt-TDDFT molecular dynamics simulations have been performed using the time-dependent ab initio package (TDAP) that can be obtained from the corresponding authors upon reasonable request. Structure and phonon calculations have been performed using VASP and PHONOPY codes that can be requested from the developers.

Received: 27 November 2022; Accepted: 7 May 2023;
Published online: 22 May 2023

REFERENCES

1. Stojchevska, L. et al. Ultrafast switching to a stable hidden quantum state in an electronic crystal. *Science* **344**, 177–180 (2014).
2. Bigot, J.-Y., Vomir, M. & Beaurepaire, E. Coherent ultrafast magnetism induced by femtosecond laser pulses. *Nat. Phys.* **5**, 515–520 (2009).
3. Nova, T., Disa, A., Fechner, M. & Cavalleri, A. Metastable ferroelectricity in optically strained $SrTiO_3$. *Science* **364**, 1075–1079 (2019).
4. Horstmann, J. G. et al. Coherent control of a surface structural phase transition. *Nature* **583**, 232–236 (2020).
5. Sokolowski-Tinten, K., Bialkowski, J. & von der Linde, D. Ultrafast laser-induced order-disorder transitions in semiconductors. *Phys. Rev. B* **51**, 14186 (1995).
6. Mo, M. et al. Heterogeneous to homogeneous melting transition visualized with ultrafast electron diffraction. *Science* **360**, 1451–1455 (2018).
7. Carbone, F., Baum, P., Rudolf, P. & Zewail, A. H. Structural preablation dynamics of graphite observed by ultrafast electron crystallography. *Phys. Rev. Lett.* **100**, 035501 (2008).
8. Sung, J. Graphite → diamond transition under high pressure: a kinetics approach. *J. Mater. Sci.* **35**, 6041–6054 (2000).
9. Mao, W. L. et al. Bonding changes in compressed superhard graphite. *Science* **302**, 425–427 (2003).
10. Luo, K. et al. Coherent interfaces govern direct transformation from graphite to diamond. *Nature* **607**, 486–491 (2022).
11. Raman, R. K. et al. Direct observation of optically induced transient structures in graphite using ultrafast electron crystallography. *Phys. Rev. Lett.* **101**, 077401 (2008).
12. Kanasaki, J., Inami, E., Tanimura, K., Ohnishi, H. & Nasu, K. Formation of sp^3-bonded carbon nanostructures by femtosecond laser excitation of graphite. *Phys. Rev. lett.* **102**, 087402 (2009).
13. Nüske, R. et al. Transforming graphite to nanoscale diamonds by a femtosecond laser pulse. *Appl. Phys. Lett.* **100**, 043102 (2012).
14. Luo, D. et al. Ultrafast formation of a transient two-dimensional diamondlike structure in twisted bilayer graphene. *Phys. Rev. B* **102**, 155431 (2020).
15. Khaliullin, R. Z., Eshet, H., Kühne, T. D., Behler, J. & Parrinello, M. Nucleation mechanism for the direct graphite-to-diamond phase transition. *Nat. Mater.* **10**, 693–697 (2011).
16. Nishioka, K. & Nasu, K. Cooperative domain-type interlayer sp^3-bond formation in graphite. *Phys. Rev. B* **82**, 035440 (2010).
17. Ohnishi, H. & Nasu, K. Generation and growth of sp^3-bonded domains by visible photon irradiation of graphite. *Phys. Rev. B* **80**, 014112 (2009).
18. Rohde, G. et al. Ultrafast formation of a Fermi-Dirac distributed electron gas. *Phys. Rev. Lett.* **121**, 256401 (2018).
19. Breusing, M., Ropers, C. & Elsaesser, T. Ultrafast carrier dynamics in graphite. *Phys. Rev. Lett.* **102**, 086809 (2009).
20. Gilbertson, S. et al. Tracing ultrafast separation and coalescence of carrier distributions in graphene with time-resolved photoemission. *J. Phys. Chem. Lett.* **3**, 64–68 (2012).
21. Bundy, F. & Kasper, J. Hexagonal diamond-a new form of carbon. *J. Chem. Phys.* **46**, 3437–3446 (1967).
22. Maultzsch, J., Reich, S., Thomsen, C., Requardt, H. & Ordejón, P. Phonon dispersion in graphite. *Phys. Rev. Lett.* **92**, 075501 (2004).
23. Piscanec, S., Lazzeri, M., Mauri, F., Ferrari, A. & Robertson, J. Kohn anomalies and electron-phonon interactions in graphite. *Phys. Rev. Lett.* **93**, 185503 (2004).
24. Kampfrath, T., Perfetti, L., Schapper, F., Frischkorn, C. & Wolf, M. Strongly coupled optical phonons in the ultrafast dynamics of the electronic energy and current relaxation in graphite. *Phys. Rev. Lett.* **95**, 187403 (2005).
25. Chatelain, R. P., Morrison, V. R., Klarenaar, B. L. & Siwick, B. J. Coherent and incoherent electron-phonon coupling in graphite observed with radio-frequency compressed ultrafast electron diffraction. *Phys. Rev. Lett.* **113**, 235502 (2014).
26. Mishina, T., Nitta, K. & Masumoto, Y. Coherent lattice vibration of interlayer shearing mode of graphite. *Phys. Rev. B* **62**, 2908 (2000).
27. Winzer, T., Knorr, A. & Malic, E. Carrier multiplication in graphene. *Nano Lett.* **10**, 4839–4843 (2010).
28. Brida, D. et al. Ultrafast collinear scattering and carrier multiplication in graphene. *Nat. Commun.* **4**, 1–9 (2013).
29. Winzer, T. & Malić, E. Impact of Auger processes on carrier dynamics in graphene. *Phys. Rev. B* **85**, 241404 (2012).
30. Plotzing, T. et al. Experimental verification of carrier multiplication in graphene. *Nano Lett.* **14**, 5371–5375 (2014).
31. Lewandowski, C. & Levitov, L. Photoexcitation cascade and quantum-relativistic jets in graphene. *Phys. Rev. Lett.* **120**, 076601 (2018).
32. Bang, J., Sun, Y., Liu, X.-Q., Gao, F. & Zhang, S. Carrier-multiplication-induced structural change during ultrafast carrier relaxation and nonthermal phase transition in semiconductors. *Phys. Rev. Lett.* **117**, 126402 (2016).
33. Fauster, T., Himpsel, F., Fischer, J. & Plummer, E. Three-dimensional energy band in graphite and lithium-intercalated graphite. *Phys. Rev. Lett.* **51**, 430 (1983).
34. Fischer, D., Wentzcovitch, R. M., Carr, R., Continenza, A. & Freeman, A. J. Graphitic interlayer states: A carbon K near-edge X-ray-absorption fine-structure study. *Phys. Rev. B* **44**, 1427 (1991).
35. Tan, S., Argondizzo, A., Wang, C., Cui, X. & Petek, H. Ultrafast multiphoton thermionic photoemission from graphite. *Phys. Rev. X* **7**, 011004 (2017).
36. Dong, X. et al. An ab initio study on the transition paths from graphite to diamond under pressure. *J. Phys. Condens. Mat.* **25**, 145402 (2013).

37. Lian, C., Hu, S.-Q., Guan, M.-X. & Meng, S. Momentum-resolved TDDFT algorithm in atomic basis for real time tracking of electronic excitation. *J. Chem. Phys.* **149**, 154104 (2018).
38. Meng, S. & Kaxiras, E. Real-time, local basis-set implementation of time-dependent density functional theory for excited state dynamics simulations. *J. Chem. Phys.* **129**, 054110 (2008).
39. Ceperley, D. M. & Alder, B. J. Ground state of the electron gas by a stochastic method. *Phys. Rev. Lett.* **45**, 566 (1980).
40. Parrinello, M. & Rahman, A. Polymorphic transitions in single crystals: a new molecular dynamics method. *J. Appl. Phys.* **52**, 7182–7190 (1981).
41. Kresse, G. & Furthmüller, J. Efficient iterative schemes for ab initio total-energy calculations using a plane-wave basis set. *Phys. Rev. B* **54**, 11169 (1996).
42. Blöchl, P. E. Projector augmented-wave method. *Phys. Rev. B* **50**, 17953 (1994).
43. Togo, A. & Tanaka, I. First principles phonon calculations in materials science. *Scr. Materialia* **108**, 1–5 (2015).

ACKNOWLEDGEMENTS

We acknowledge partial financial support from the National Key Research and Development Program of China (No. 2021YFA1400503, 2021YFA1400201), National Natural Science Foundation of China (No. 12025407, 11774396 and 11934003, 11974400), and "Strategic Priority Research Program (B)" of Chinese Academy of Sciences (Grant No. XDB330301). M.G. acknowledges support from the China Postdoctoral Science Foundation (Grant No. 2021M693369).

AUTHOR CONTRIBUTIONS

C.S. and M.G. contributed equally. C.Z. and S.M. designed and directed the study. The calculations were mainly performed by C.S. The paper was written by C.S., M.G., C.Z., and S.M. All authors contributed to the discussions and analyses of the data, and approved the final version.

COMPETING INTERESTS

The authors declare no competing interests.

ADDITIONAL INFORMATION

Supplementary information The online version contains supplementary material available at https://doi.org/10.1038/s41524-023-01035-2.

Correspondence and requests for materials should be addressed to Cui Zhang or Sheng Meng.

Reprints and permission information is available at http://www.nature.com/reprints

Publisher's note Springer Nature remains neutral with regard to jurisdictional claims in published maps and institutional affiliations.